

# Tunable Indistinguishable Photons From Remote Quantum Dots

R. B. Patel,<sup>1,2,3</sup> A. J. Bennett,<sup>1,3,\*</sup> I. Farrer,<sup>2</sup> C. A. Nicoll,<sup>2</sup> D. A. Ritchie,<sup>2</sup> and A. J. Shields<sup>1</sup>

<sup>1</sup>*Toshiba Research Europe Limited, Cambridge Research Laboratory,  
208 Science Park, Milton Road, Cambridge, CB4 0GZ, U. K.*

<sup>2</sup>*Cavendish Laboratory, Cambridge University,  
JJ Thomson Avenue, Cambridge, CB3 0HE, U. K.*

<sup>3</sup>*These authors contributed equally*

(Dated: October 22, 2018)

## Abstract

Single semiconductor quantum dots have been widely studied within devices that can apply an electric field. In the most common system, the low energy offset between the InGaAs quantum dot and the surrounding GaAs material limits the magnitude of field that can be applied to tens of  $\text{kVcm}^{-1}$ , before carriers tunnel out of the dot. The Stark shift experienced by the emission line is typically  $\sim 1$  meV. We report that by embedding the quantum dots in a quantum well heterostructure the vertical field that can be applied is increased by over an order of magnitude whilst preserving the narrow linewidths, high internal quantum efficiencies and familiar emission spectra. Individual dots can then be continuously tuned to the same energy allowing for two-photon interference between remote, independent, quantum dots.

PACS numbers: 78.67.-n, 85.35.Ds

---

\*Electronic address: anthony.bennett@crl.toshiba.co.uk

In recent years self-assembled semiconductor quantum dots have been established as one of the most versatile systems for studying quantum effects in the solid-state as well as quantum optics. A plethora of quantum dot based field-effect devices have been developed which allow controlled charging of a quantum dot[1], Rabi oscillations[2], coherent spin control[3] and electrically injected non-classical photon emission[4]. Often referred to as “artificial atoms”, quantum dots possess discrete energy levels which make them a viable candidate for qubits. However, unlike single atoms, no two quantum dots are alike and experiments are often limited due to the distributions in energy, fine-structure and linewidths in which they form. This is a complication for quantum information applications that require qubits to be initialized in the same state. Furthermore, distributed quantum computing requires interactions between remote qubit systems mediated by indistinguishable photons. Quantum effects between remote sources have been observed with ions[5, 6], atoms[7, 8] and parametric down-conversion[9, 10] in which photons are naturally generated with the same energy. Recently, quantum interference has been demonstrated between donor impurities on the same chip[11]. Though in this case the visibility of interference is hampered by a lack of control over the emission energy and unfavorable multi-photon emission. It would be desirable to be able to precisely engineer the characteristics of each emitter independently.

Consider the probability of finding two quantum dots with the same transition energy. Typically, the distribution of energies in a sample can be as low as 10 meV, however the narrowest linewidths tend to range from 1 – 5  $\mu\text{eV}$ [12, 13]. Therefore there is a minute chance of finding two dots with perfectly overlapping spectra. Perhaps the easiest method of tuning the transition energy is by applying a vertical electric field, however, tunneling of carriers out of the dot results in a Stark shift of only  $\sim 1$  meV before the emission is quenched[14, 15]. We circumvent this issue by embedding our quantum dots in the center of a GaAs/AlGaAs quantum well. Not only does this retain the favorable properties of the InGaAs/GaAs quantum dot system, but it also allows carrier confinement even in the presence of large vertical electric fields leading to energy shifts of up to 25 meV. We demonstrate these states are quantum mechanically identical by carrying out two-photon interference between photons emitted by remote quantum dots.

To begin with, we shall briefly discuss our samples. The first, which we denote Dot A, constitutes our reference sample and is an electrically injected InAs quantum dot embedded in a microcavity p-i-n diode. Previous studies of this sample have shown a low multi-photon

emission probability, narrow linewidth and bright electroluminescence (EL). The emitting state is a negatively charged exciton ( $X^-$ ) emitting at 1.314 eV. This state has exhibited a high degree of indistinguishability between consecutively emitted photons and also with a coherent laser[16]. The second set of samples consist of a single layer of InAs quantum dots embedded in the center of a 10 nm GaAs quantum well clad with  $\text{Al}_{0.75}\text{Ga}_{0.25}\text{As}$ . These layers encompass a half-wavelength thick cavity between two Bragg reflectors. The microcavity serves to enhance the photon collection efficiency with negligible effect on the emission rate. The indium deposition and layer thicknesses of the microcavity were tailored for emission at around 1.314 eV. Doping was introduced allowing a vertical electric field to be applied. A schematic of the band structure is shown in Fig. 1a. Single dots were isolated using an array of apertures patterned in the top contact of the device. Common to nearly all single quantum dots is the change in the carrier occupancy as a function of effective field  $F$  (Fig. 1b). Exciton ( $X$ ), biexciton ( $XX$ ) and charged exciton ( $X^-$ ,  $X^+$ ) states can be identified. Each state shifts in a parabolic fashion with fields up to  $-500 \text{ kVcm}^{-1}$ . This is an order of magnitude increase over previously reported values where  $60 \text{ kVcm}^{-1}$  fields would result in quenching of the emission[14, 15]. Stark shifts of up to 25 meV have been observed for single  $X$  states, with measured polarizabilities and dipole moments consistent with data reported with much smaller fields[17]. Although some selectivity is applied to identify the brightest and narrowest lines we find most dots can be tuned to the target energy of 1.314 eV. Below we utilize the  $X^-$  states of the dots.

In Fig. 1c we demonstrate tuning of two quantum dot  $X^-$  states to the same energy. In this case, the tunable dot (Dot 1) emits at the target energy of 1.314 eV with a net field of  $-50 \text{ kVcm}^{-1}$ . High-resolution spectroscopy (Fig. 1d) with a scanning Fabry-Pérot interferometer ( $0.8 \mu\text{eV}$  resolution) allows us to tune the two states to degeneracy. Dot A, reveals a Lorentzian lineshape with a FWHM of  $5.2 \mu\text{eV}$ . Dot 1 however is best fitted with a Voigt profile with a homogenous linewidth of  $2.2 \mu\text{eV}$  and a Gaussian width of  $6.8 \mu\text{eV}$ . We note that most lines in other dots exhibit a predominantly Lorentzian lineshape.

To further demonstrate the control we have over the energy, we now discuss two-photon interference measurements taken with these two dots. Two-photon interference refers to the phenomena whereby single photons entering a 50:50 beamsplitter from opposite inputs “coalesce” and exit together, provided they are indistinguishable[18]. This is also used as a test of purity of a quantum light source[12, 19, 20]. Both samples were held in two separate

cryostats located 1.1 m apart at 4.5 K. For Dot A the device was held at a fixed bias corresponding to a current of 130  $\mu\text{A}$ , whilst Dot 1 was excited with a continuous-wave laser emitting at 1.459 eV. These conditions were chosen to give equal intensity, bright emission from each sample whilst also maintaining narrow linewidths. Emission from each dot is directed into a polarizing beamsplitter (Fig. 2) where the orthogonally polarized, co-parallel, beams are spectrally filtered using a monochromator. They are then coupled into a custom-built Mach-Zehnder interferometer made out of polarization-maintaining single-mode fiber. A polarizing coupler separates the emission from each source and sends them along individual paths onto a 50:50 coupler. We periodically rotate the paths from being mutually parallel in polarization (indistinguishable) or orthogonal in polarization (distinguishable). We thereby build correlations for both cases during the same experimental run, canceling any effects due to drift. Photons are detected using two silicon avalanche photodiode detectors,  $D_1$  and  $D_2$ . The temporal response of the system  $R_f$  is a Gaussian with a FWHM of 428 ps.

First we determine the multi-photon emission probability for each source. These were measured in a Hanbury-Brown and Twiss experiment by blocking the emission from one of the sources whilst measuring the second-order correlation for the other. The data in Fig. 3a and b were fitted with the function  $g^{(2)}(\tau) = R_f \otimes (1 - (1 - B)\exp(-|\tau|/\tau_r))$  where  $\tau$  is the time between detections,  $B$  is the background contribution and  $\tau_r$  is the radiative lifetime of the source. The blue curves in each figure are fits assuming an infinitely fast response,  $B = 0.05$  and  $\tau_r = 600$  ps for Dot A, and  $B = 0$  and  $\tau_r = 800$  ps for Dot 1. Convolution with the known response of our detectors (red curve) results in an excellent fit to the data.

In Fig. 3c and d we present interference data where the energy detuning of Dot 1 from Dot A,  $\Delta E = 0$   $\mu\text{eV}$ , and each source delivers photons with parallel polarization and orthogonal polarization respectively. The signature of two-photon interference is a difference in the depth of the dip at  $\tau = 0$  ns. For orthogonally polarized photons, the photons are distinguishable and no interference occurs. Therefore, there is equal chance of the two photons exiting the beamsplitter in the same direction or in opposite directions result in a dip to 50%. Indistinguishable photons with parallel polarization give rise to interference leading to a suppression in coincident counts and a dip to 0%. For each measurement the dip does not reach the ideal values of 0% and 50% respectively, due to the response of our detectors. We have developed a model to account for this and also the difference coherence times, beamsplitter coefficients, imperfect wavepacket overlap  $\gamma = \langle \psi_A | \psi_1 \rangle$ , and finite multi-

photon emission  $g^{(2)}(0)$  for each source. We also account for the Gaussian component of Dot 1 numerically by including a spectral jitter in the emission energy whose magnitude is determined from a Voigt fit of the spectra. As a measure of mutual indistinguishability between the two sources, we define the visibility of two-photon interference as  $V = (g_{\perp}^{(2)}(\tau) - g_{\parallel}^{(2)}(\tau))/g_{\perp}^{(2)}(\tau)$ . By post-selecting events where photons arrive simultaneously at the final coupler, we measure a visibility of  $33 \pm 1\%$  from the raw data (Fig. 3e) which agrees with our model. As shown by the blue curve, without the limitation of timing resolution it should be possible to achieve a visibility of up to 98%.

Scaling a system to multiple qubits is an important requirement for realizing many useful applications in quantum information processing. Linear optical schemes using quantum dots would greatly benefit from the ability to interfere photons from arrays of quantum dots in separate locations. Our technique can be used to tune a number of quantum dots to the same energy. We demonstrate this with our devices by repeating the interference measurements for two other dots. High-resolution PL measurements of Dot 2 and 3 indicate a Lorentzian lineshape and negligible inhomogeneous broadening. Table 1 provides a summary of these results where in each case we infer an overlap close to unity. This shows that we can observe interference with a visibility that can be determined from independent Hanbury-Brown and Twiss and coherence time measurements. This ability to produce many indistinguishable quantum states in remote solid-state systems is required for quantum communication networks and distributed quantum computing.

Control over the emission energy allows us to perform an experiment analogous to the famous ‘‘Hong-Ou-Mandel dip’’ experiment in which a rate of coincidences is recorded as some distinguishing character is introduced between photons. Conventionally, this is achieved by delaying a photon in time relative to another[18, 19, 20]. In our experiment we introduce a controllable energy difference between Dot A and Dot 1 and measure the visibility of interference which is shown in Fig. 3f. Notice that a high degree of interference is only seen when  $\Delta E$  is close to zero. For two sources that are homogeneously broadened, it can be shown that the width of the peak in Fig. 3f should be equal to the sum of the linewidths of the two sources (in the limit where the coherence time is much less than the radiative lifetime and detection resolution). Our model predicts a similar width of  $15 \mu\text{eV}$ . In contrast, the experiment reveals a peak of width  $4.9 \mu\text{eV}$ . This suggests that for finite detunings the sources are more distinguishable than is suggested by their spectra. This would be

the case if information about the emitted photons were retained by the sources after emission, for instance if a given photon had a narrower linewidth than that observed in the time-averaged spectra. Such an observation is outside the scope of the accepted models of two-photon interference[21] but we hypothesize that this information is retained by the solid-state environment around the quantum dot after radiative recombination from the  $X^-$  state, for example in the fluctuations that lead to inhomogeneous broadening of the dot. An interesting way to test this would be to probe the environment directly using a single shot absorption technique immediately after the photon is emitted. In future higher visibilities of interference could be achieved using pulsed[20] or resonant excitation[13].

The ability to apply large electric fields to single quantum dots, whilst maintaining high quantum efficiencies, provides a major step towards refining quantum dot based single-photon sources. The high degree of control over the transition energy we have shown solves the long standing problem of identifying quantum dots with the same energy. Thus allowing, for the first time, two-photon interference between remote quantum dots. Experimental measurements of the interference visibility are in agreement with our predictions for the three pairs of quantum dots studied showing that a large degree of overlap is achievable between photons emanating from different dots. This work opens up the possibility of transferring quantum information between multiple, remote, sources in the solid-state.

This work was partly supported by the EU through the IST FP6 Integrated Project Qubit Applications (QAP: contract number 015848). EPSRC provided support for RBP and QIPIRC for CAN.

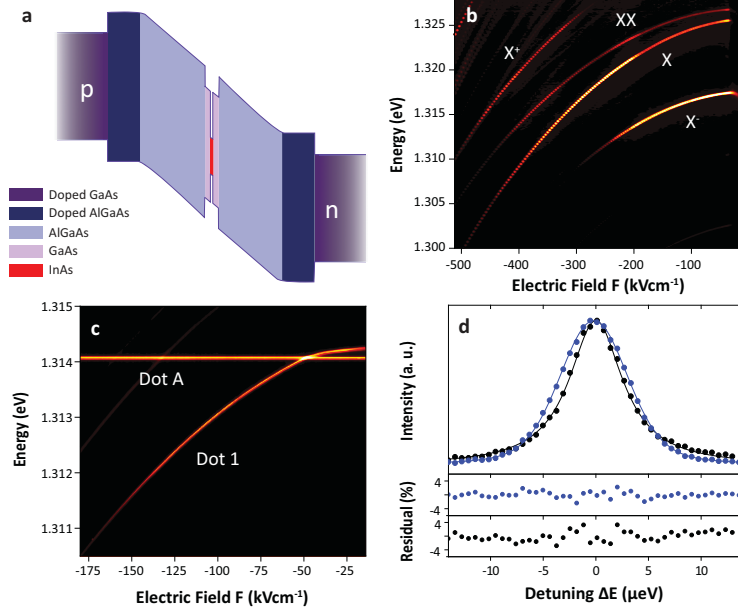


FIG. 1: Design and spectral characteristics of our tunable source. (a) Schematic illustrating the band structure near the active region of the tunable device. A layer of InAs quantum dots is grown at the center of a 10 nm GaAs quantum well clad with a  $\text{Al}_{0.75}\text{Ga}_{0.25}\text{As}$  short period superlattice. (b) Typical spectra of a single quantum dot as the field is varied. The states are identified as exciton ( $X$ ), biexciton ( $XX$ ) and charged exciton ( $X^-$ ,  $X^+$ ). (c) Tuning Dot A and Dot 1 to the same energy. (d) High-resolution spectra of Dot A (black circles) and Dot 1 (blue circles) at zero detuning. A Lorentzian spectrum (black curve) is observed for Dot A with a linewidth of  $5.2 \mu\text{eV}$ . Dot 1 shows a Gaussian component and is fitted with a Voigt profile (blue curve). Also shown are the residuals of the least-squares fit.

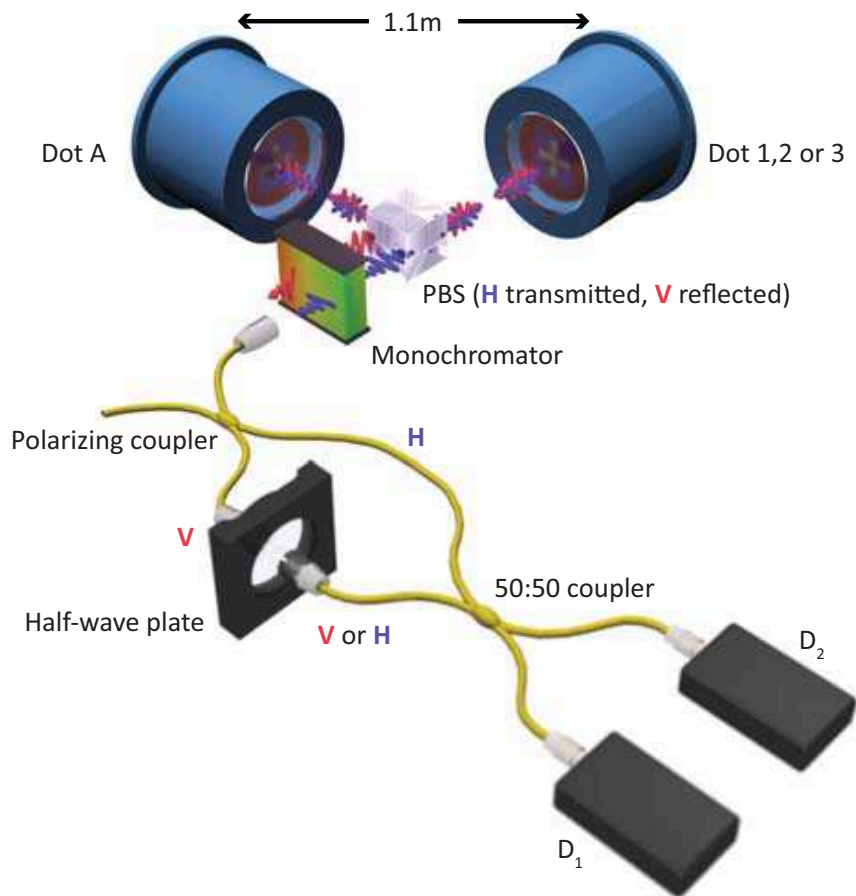


FIG. 2: Experimental arrangement for two-photon interference. The two sources are located 1.1 m apart. V polarized photons from Dot A and H polarized photons from Dot 1,2 or 3 are collected and filtered using a monochromator. The emission is coupled into a Mach-Zehnder interferometer made from polarization-maintaining single-mode fiber. Emission from the individual sources is separated using a polarizing coupler and then brought together in a 50:50 coupler. Correlations are recorded whilst periodically switching a half-wave plate making the photons mutually indistinguishable or distinguishable.



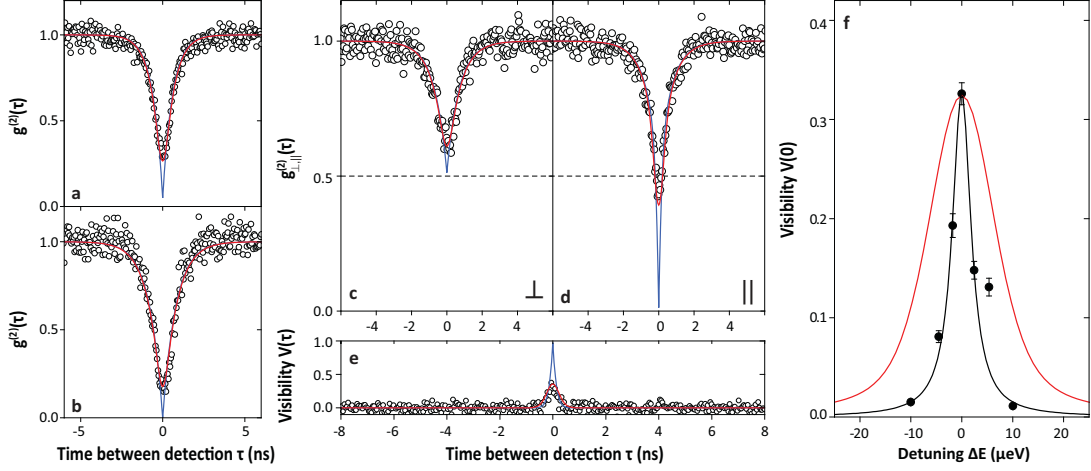


FIG. 3: Hanbury-Brown and Twiss and two-photon interference results. In (a)-(f) blue curves correspond to fits assuming unlimited timing resolution and red curves to fits assuming a Gaussian response of 428 ps. (a) Autocorrelation for Dot A, with  $g^{(2)}(0) = 5\%$ . (b) Autocorrelation for Dot 1, with  $g^{(2)}(0) = 0\%$ . (c-d) Two-photon interference measurements with  $\Delta E = 0 \mu\text{eV}$ . (c) With mutually orthogonal polarized photons the dip is above the classical limit (dashed line) and no interference has occurred. (d) Parallel polarized photons result in a dip below the 50 % owing to two-photon interference. (e) Raw interference visibility limited mainly by the timing resolution. (f) Measurements of visibility as a function of  $\Delta E$  fitted with our model (red line) and with a Lorentzian with  $\text{FWHM} = 4.9 \mu\text{eV}$  (black line)

Dot	Dot A properties			Tunable dot properties			V (%)	Predicted V (%)
	Current ( $\mu\text{A}$ )	Linewidth ( $\mu\text{eV}$ )	$g^{(2)}(0)$ (%)	F ( $\text{kVcm}^{-1}$ )	Linewidth ( $\mu\text{eV}$ )	$g^{(2)}(0)$ (%)		
1	130	5.1	5	-50.0	2.2 (L), 6.8 (G)	0	$33 \pm 1$	33
2	150	6.4	10	-98.8	10.8	0	$18 \pm 2$	20
3	100	4.5	0	-61.9	7.9	0	$32 \pm 6$	27

FIG. 4: Summary of interference results for Dot A and 1-3. Labels L denotes lorentzian lineshapes, and G denotes Gaussian lineshapes.

- 
- [1] R. Warburton *et al.* Nature **405**, 926 (2000).
  - [2] A. Zrenner *et al.* Nature **418**, 612 (2002).
  - [3] M. Atature *et al.* Science **312**, 551 (2006).
  - [4] Z. Yuan *et al.* Science **295**, 102-105 (2002).
  - [5] P. Maunz *et al.* Nat. Phys. **3**, 538-541 (2007).
  - [6] S. Olmschenk *et al.* Science **323**, 486 (2009).
  - [7] J. Beugnon *et al.* Nature **440**, 779-782 (2006).
  - [8] T. Chaneliere *et al.* Phys. Rev. Lett. **98**, 113602 (2007).
  - [9] R. Kaltenbaek *et al.* Phys. Rev. Lett. **96**, 240502 (2006).
  - [10] M. Halder *et al.* Nat. Phys. **3**, 692-695 (2007).
  - [11] K. Sanaka *et al.* arXiv:0903.1849 (2009).
  - [12] R. Patel *et al.* Phys. Rev. Lett. **100**, 207405 (2008).
  - [13] S. Ates *et al.* Phys. Rev. Lett. **103**, 167402 (2009).
  - [14] R. Oulton *et al.* Phys. Rev. B. **66**, 045313 (2002).
  - [15] F. Findeis *et al.* Appl. Phys. Lett. **78**, 2958 (2001).
  - [16] A. Bennett *et al.* Nature Phys. **5**, 715 (2009).
  - [17] J. Finley *et al.* Phys. Rev. B. **70**, 201308 (2004).
  - [18] C. Hong *et al.* Phys. Rev. Lett. **59**, 2044-2046 (1987).
  - [19] C. Santori *et al.* Nature **419**, 594-597 (2002).
  - [20] A. Bennett *et al.* Appl. Phys. Lett. **92**, 193503 (2008).
  - [21] T. Legero *et al.* Phys. Rev. Lett. **93**, 070503 (2004).